NUMERICAL SIMULATION AND OPTIMIZATION OF THE CASTING PROCESS OF A CASTING-STEEL WHEEL

G. Mi[1*] – C. Li[1] – Y. Liu[1] – B. Zhang[2] – G. Song[3]

[1]School of Materials Science and Engineering, Henan Polytechnic University, Henan, Jiaozuo, 454003, P.R. China
[2]Metals and Chemistry Institute, China Academy of Railway Sciences, Beijing, 10081, P.R. China
[3]Datong ABC Casting Co. Ltd, Technology & Quality Department, Shanxi, Datong, 037038, P.R. China

ARTICLE INFO

***Article history*:**
Received 8.11.2012
Received in revised form 2.12.2012
Accepted 3.12.2012

Keywords:
Cast-steel wheel
Solidification simulation
Foundry technique
Heat insulating material

Abstract:

The mechanism of formation and the regularity of shrinkage distribution in a cast-steel wheel were simulated by computer methods. SolidWorks software package was used to produce a three-dimensional model of the cast parts, and Experto ViewCast software package was employed to simulate the casting process. The simulated results show that the mold filling was smooth and thus no splashing occurred. However, shrinkage and porosity appeared at the transition phase between the wheel-rim and web during the process of solidification. The reason for that is the imperfect solidification sequence. The fast cooling rate in the final thin web position led to the block of feeding channel at the transition area. The foundry technique was improved successfully by computer-aided methods. The volume of shrinkage was reduced by applying an insulating material, which made the castings solidify progressively as designed. The performance of the wheel produced by the improved technology agreed very well with the technical requirements.

1 Introduction

To improve the transport abilities of railway freight cars, the speed and the hauling capacity are the quantities that must be increased. Increasing the axle load is an important step in the development of freight transportation that increases traffic income and reduces the maintenance costs. As the key components of the rail truck, wheels are related to the safety of rail transportation. Hence, the wheel is the key point following the increasing of speed and axle load [1,2,3].

There are two kinds of wheels in freight cars at present: the rolled-steel wheel and cast-steel wheel. The rolled-steel wheel is manufactured by rolling the ingot again and again, and the cast-steel wheel is manufactured by casting. Generally, the plasticity and ductility of the rolled-steel wheel exceeds those of cast-steel wheel. However, in freight transport running conditions, the service performance of the cast-steel wheel is in general commensurate with that of the rolled-steel wheel. The cast-steel wheel has been approved around the world because of the short process flow, simple technology, low cost and high foundry accuracy associated with their production [4,5]. In addition, the cast-steel wheel has gradually occupied an important domestic truck market, showing a growth trend in this area.

* Corresponding author. Tel.: + 86 391 3987503; fax: + 86 391 3987503
E-mail address: peter@hpu.edu.cn

The cross sectional dimensions of cast-steel wheels vary in a wide range and shrinkage is easily generated in the transition area between the wheelrim and the web during manufacture. The shrinkage in this area is an urgent problem. After numerical simulations have been employed in this research to analyze the formation process, and the genesis and location of the defects determined, then the foundry technique can be optimized based on these results.

2 Simulation analysis

2.1 Geometry

The 3-D geometries are created by Solid-Works 3-D software and the drawings are saved as the format of *.STL. The wheel casting geometry is shown in Fig. 1. The 3-D models (STL format) are then imported into Experto ViewCast software which is used for numerical simulation and design and developed by SIRRIS Foundry Center in Belgium. The importing sequence is: graphite - sand lining - casting - core - float core. The mesh adopted was hexahedral with a total number of 4 millions, which were divided by the self-module of ViewCast.

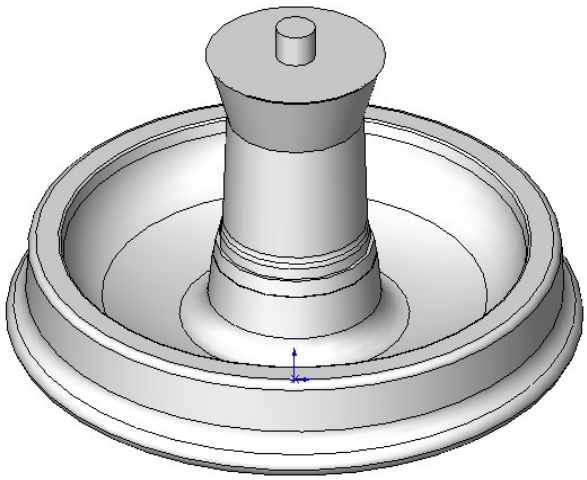

Figure 1. Casting geometry.

2.2 Materials and technology

ZL-B is used for the wheel steel. The chemical composition of ZL-B is shown in Table 1. The gross weight of the casting is approximately 430 kg. The initial conditions and solidification boundary conditions are determined according to the actual processing parameters. The preheating temperature of the mold is 150 °C, and the pouring temperature is 1560 °C.

3 Technology design

Scheme I: The mold consists of graphite, a sand lining and a core. The wheel rim, wheel flange and wheel tread are all directly in contact with the graphite. The mold sand and core sand are chemically bonded sands. A deluge system was used as a gating system. The pouring cup also acts as a riser. The advantage of this system is that the casting yield can be increased. The assembly is shown diagrammatically in Fig. 2.

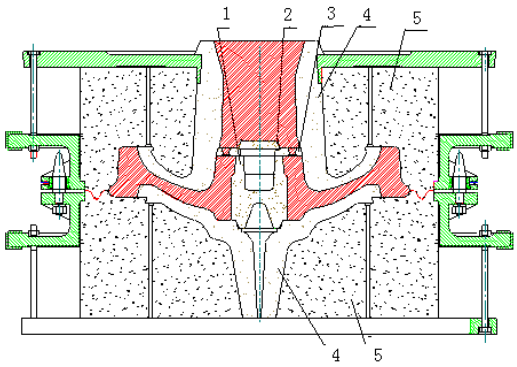

Figure 2. Mold assembly diagram: 1-middle core, 2-float core, 3-deluge core, 4-sand lining, 5-graphite.

Scheme II: Based on scheme I, an 8-mm-thick layer of heat insulating material is added and the corresponding shape is shown in Fig. 3.
Scheme III: Based on scheme II, the heat insulation material is moved a distance of 5 mm towards inside direction, and the thickness of heat insulation material increased by 2 mm.

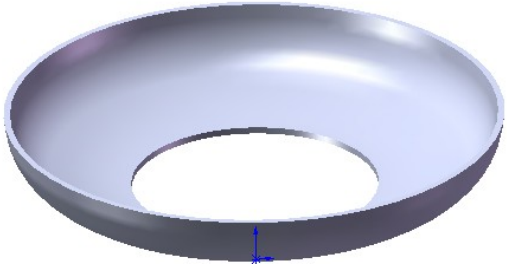

Figure 3. Geometry of the insulation material.

Table 1. Composition of the cast-steel wheel material (w_B%)

C	Si	Mn	P	S	Cr	Ni	Mo	Cu	V	Al	Fe
0.57-0.67	0.15-0.37	0.60-0.85	≤0.035	≤0.040	≤0.25	≤0.25	≤0.10	≤0.35	≤0.04	≤0.06	Rest

4 Simulation results and discussions

4.1 Mold filling of scheme I

The simulation results of the mold filling of scheme I are shown in Fig. 4. The molten metal flowed from the pouring cup along the pop gates, and while entering the cavity it separated into twelve strands, reducing thus the shock to the mold. The molten metal first filled up the pouring cup owing to the blockage of the pop gate. When the filling volume was 25%, the molten metal began to fill the wheel web smoothly from the bottom. When the filling volume reached 55%, the molten metal flowed from the web and entered the wheel-rim location. The metal exhibited some fluctuation because the wheel rim is lower than the web, but it did not splash. The metal then filled the entire cavity smoothly. Throughout the entire process, the horizontal liquid level of the cavity was being simultaneously filled, which is beneficial for inclusion and slag rising. This mold filling process is acceptable.

4.2 Solidification procedure of scheme I

The solidification simulation is proceeded by using the temperature field just after mold filling. Fig. 5 shows the solidification results and the color bar indicates the solidification time(s). The transparent body indicates the frozen mental.

From Fig. 5, it can be observed that the tread, flange and rim in contact with the graphite are the first to solidify, and then the rest of the material gradually solidified progressing toward the wheel hub. The dimension from the wheel rim to the web changes sharply, therefore, this transition is the thinnest area. When the solidification time was t = 470 s, the thinnest location began to solidify prior to its surroundings. It totally solidified at t = 525 s, leading to isolated islands in the transition area. During solidification, these isolated islands form some shrinkage defects. After 4100 s, the casting solidified completely, and the wheel hub was the last area to solidify. Viewing the whole solidification, the wheel is not well described by progressive solidification.

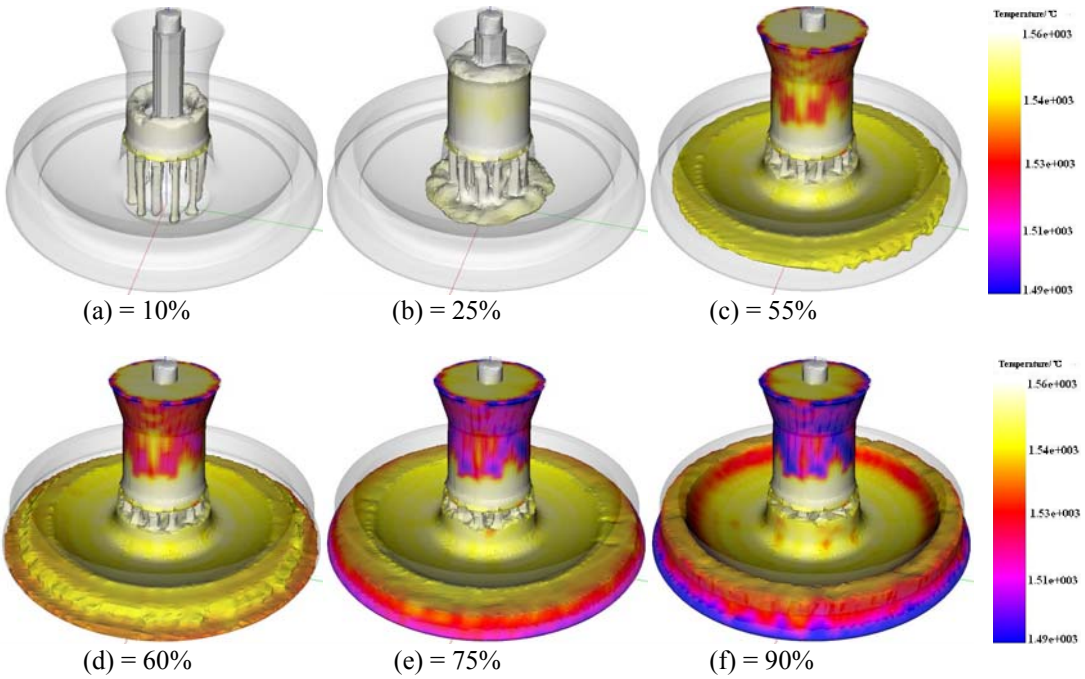

Figure 4. Simulation results of the filling process in scheme I.

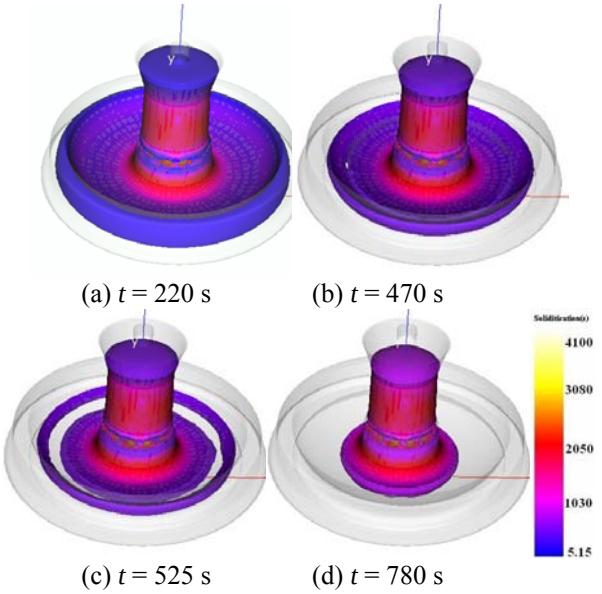

(a) t = 220 s (b) t = 470 s

(c) t = 525 s (d) t = 780 s

Figure 5. Simulation results of the solidification process in scheme I.

Fig. 6 shows the solid fraction of the wheel at t = 525 s, at the middle cross section. The cooling velocities of the thinnest location (point 1) and the wheel rim (point 3) were somewhat faster than that of the transition area (point 2), causing a non-homogeneous temperature gradient. When point 1 and point 3 solidified, point 2 was still in a liquid phase. The riser cannot feed this zone during further solidification, and therefore it results in shrinkage defects. Fig. 7 shows the temperature distribution curve at the middle cross section. Test point 1 was located at the wheel tread, and test point 14 was located at the wheel hub center. Test point 8 is the thinnest location, located at point 1 in Fig. 6. The temperature at test point 8 is lower than that of the surroundings. The temperature D-value can reach 30°C, so this position cools faster.

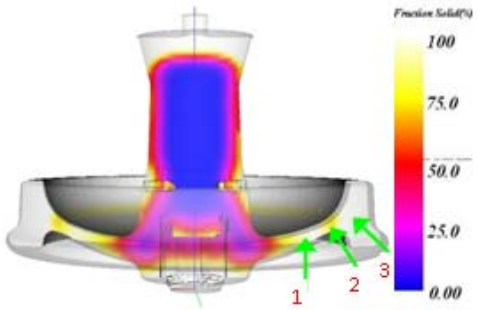

Figure 6. Simulated fraction solid distribution in scheme I.

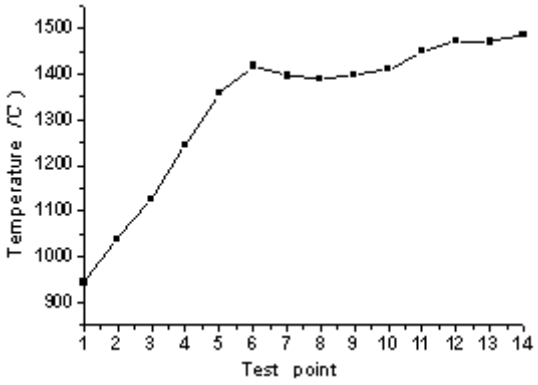

Figure 7. Temperature distribution curve of the wheel section in scheme I (t = 525 s)

Fig. 8 shows the defect distribution after the total solidification of the wheel, where (a) shows shrinkage distributions when a metal content lower than 97% is considered as a defect and (b) shows shrinkage distributions when a metal content lower than 90% is considered as a defect.

Shrinkage defects mainly appeared at the locations of isolated islands and the hub that was the last to solidify. The shrinkage at the hub can be removed after machining. Thereby, these defects affect the wheel properties concentrated in the transition area from the wheel rim to the web. During solidification, the liquid contraction and the liquid-solid contraction are the main contributors to the shrinkage. If the feeding passage is open and there is no interdendritic framework, the liquid-solid contractions can be compensated by the feeders. While the feeding passage is blocked, the liquid is separated and enclosed by a dendrite, and the liquid-solid contractions will generate shrinkage porosity. The liquid-solid contraction coefficient is the indicator for the shrinkage formation [6, 7].

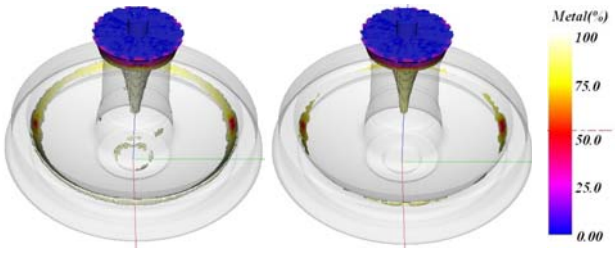

(a) Metal content lower than 97%

(b) Metal content lower than 90%

Figure 8. Simulated shrinkage distribution of scheme I.

4.3 Solidification procedure of scheme II

The improvement of the technology has no influence on the mold filling, so only solidification calculations are carried out in scheme II and scheme III.

As discussed earlier, the main reason for the formation of shrinkage is that the thinnest location cools faster than the surroundings, blocking the feeding path. Thereby, a heat insulating material was employed in scheme II to prolong the solidification time of the thinnest part and keep the feeding path open.

The simulation results are shown in Fig. 9. The casting realized a proper solidification sequence.. Solidification started from the wheel tread and extended to the hub center. During solidification, no isolated islands appeared, and the temperature gradient changed gradually. Fig. 10 shows the temperature distribution of the wheel at t = 750 s, at the middle cross section. The slope increased gradually, with only a small fluctuation at point 5, and continued to increase up to the peak. The heat insulating material was effective in scheme II; it changed the temperature distribution of the wheel during solidification, and the casting was fed well.

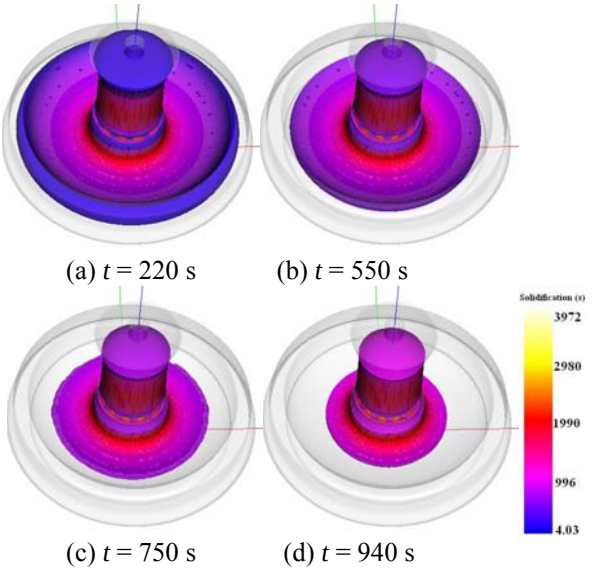

(a) t = 220 s (b) t = 550 s

(c) t = 750 s (d) t = 940 s

Figure 9. Simulation results of the solidification process in scheme II.

Fig. 11 shows the defect distribution of scheme II. It is clear that the shrinkage was greatly reduced and that there were hardly any defects in Fig. 11 (b). The simulation results of scheme II are superior to those of scheme I.

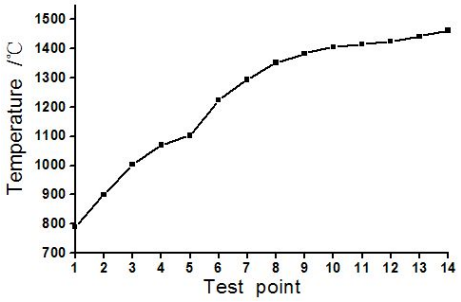

Figure 10. The temperature distribution curve of the wheel section in scheme II (t=750 s).

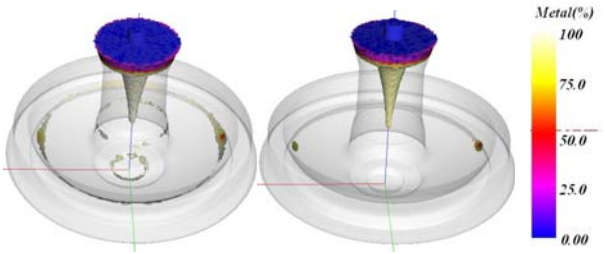

(a) Metal content lower than 97% (b) Metal content lower than 90%

Figure 11. Simulated shrinkage distribution of scheme II.

4.4 Solidification procedure of scheme III

In scheme II, the heat insulating material is in direct contact with the casting and the well insulated material. However, owing to the intrinsic heat insulating characteristics of the material, the casting surface quality will decline sharply, affecting the extrinsic features and usage. To ensure the surface quality of the casting, the heat insulating material is moved to the sand lining and the thickness is increased in scheme III.

Fig. 12 shows the simulation results of scheme III. It can be observed that the insulation effect in scheme III is reduced compared with that of scheme II. The casting solidification edge appeared scattered over an area solidifying at t = 730 s, and then the sequence of solidification restarted toward the hub center. Fig. 13 shows the wheel section temperature distribution at t = 730 s. 9 point test is at the bottom of the curve, and the temperature difference is 2 °C relative to 8 point test and only 7 °C relative to 10 point. Test. The solidification process was nearly sequential. Fig. 14 shows the defect distribution of scheme III. Compared with scheme II, the solidification results of scheme III are slightly worse,

though they are better than those of scheme I. Considering all aspects, the design of scheme III is superior to that of scheme II.

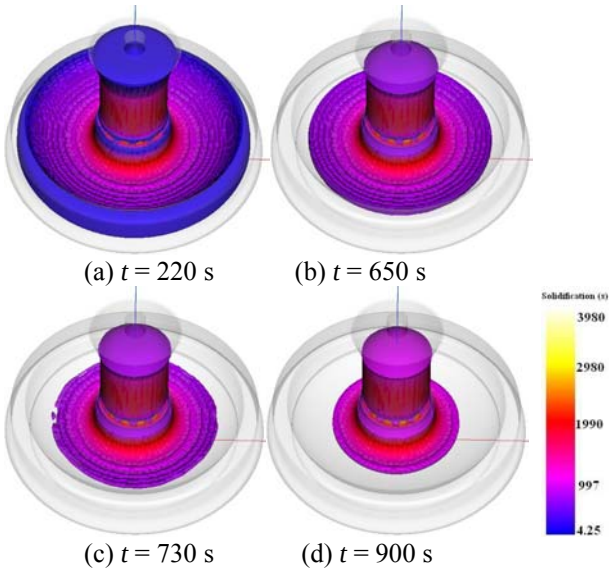

(a) t = 220 s (b) t = 650 s

(c) t = 730 s (d) t = 900 s

Figure 12. Simulation results of the solidification process in scheme III.

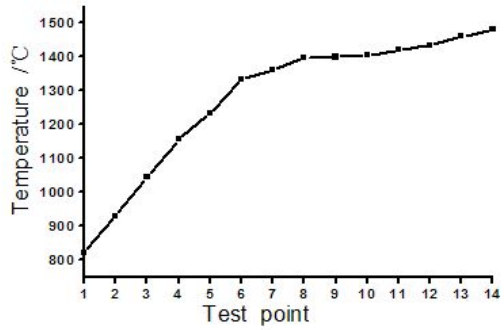

Figure 13. Temperature distribution curve of the wheel section in scheme III (t=730 s).

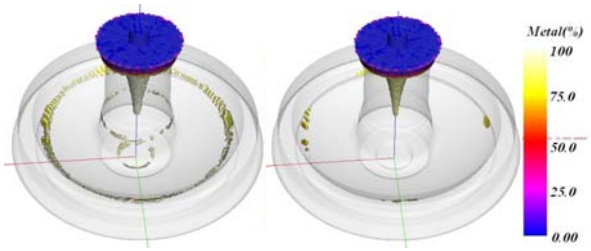

(a) Metal content lower than 97% (b) Metal content lower than 90%

Figure 14. Simulated shrinkage distribution of scheme III.

5 Actual production

Fig. 15 shows a wheel manufactured by the improved technology. The microstructure is pearlite with a small amount of reticular ferrite, as shown in Fig. 16. According to the documented standards [8], the macrostructure characterization and the fault detection were carried out on the wheel's middle section, as shown in Fig. 17. Fig. 18 shows the familiar macrostructure defect [9]. No fisheyes, cracks, impurities, shrinkage or separation were found in the results, and the wheel met all technical requirements easily.

Figure 15. The cast-steel wheel product.

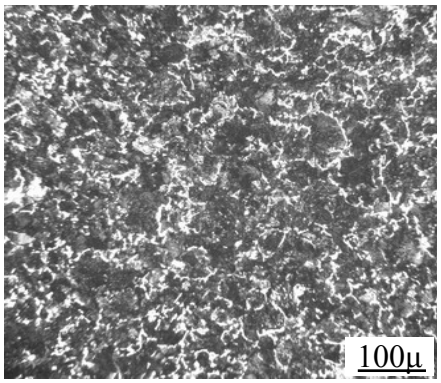

Figure 16. Microstructure of the cast-steel wheel.

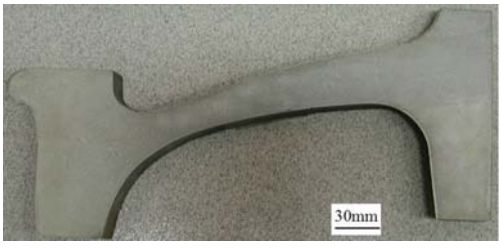

Figure 17. Macrostructure of the wheel section.

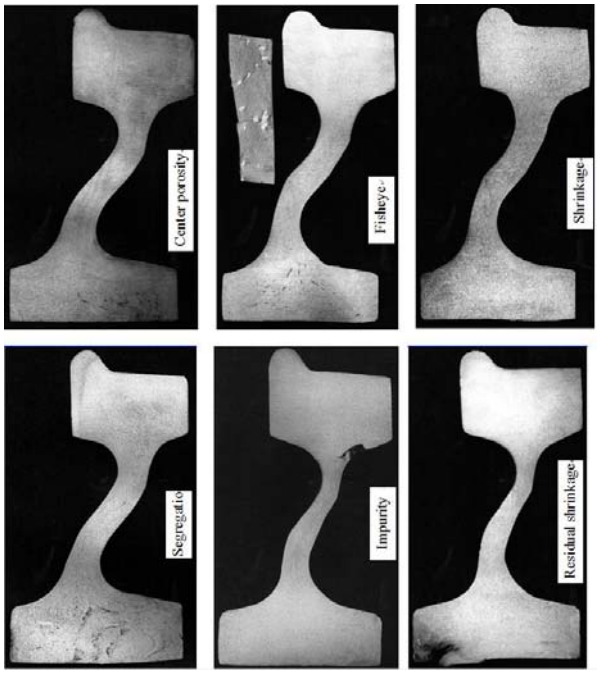

Figure 18. Macrostructure defects of the wheel

6 Conclusion

(1) The simulation results of scheme I indicated that the mold filling was smooth and that no splashing occurred. However, during the solidification process, shrinkage and porosity appeared in the transition zone of the wheel rim and web. The reason for that is the imperfect solidification sequence.
(2) The simulation results of scheme II and scheme III indicated that the solidifying order/sequence could be improved by adding a layer of heat insulating material, and the defects in the cast disappeared largely. Considering the intrinsic heat insulating material and the surface quality of the cast, scheme III was the optimal design.
(3) The defect location can be predicted by numerical simulation. The solidifying sequence can be improved by using heat insulating materials and defects in the product can be eliminated. Other properties of the wheel have also met all technical requirements.

References

[1] Song, G.X., Wang, Z.G., Dai, Y.K.: *Test and research on the abrasion resistance and contact fatigue performance of the material of ZL-B cast steel wheels*, Rolling Stock, 42 (2004), 9-11 (in Chinese).
[2] Liu, R.T., Liu, W.B., Liu, J.Y.: *Engineering Material Mechanical Property*, Harbin Institute of Technology Press, Harbin ,2001 (in Chinese).
[3] Pashlok, I.L.: *Improvement of wheel hardness,* Foreign Rolling Stock, 38 (2001), 41-44.
[4] Zhang, B., Chen, L.: *Development of wheel technology on railway freight car in China*, Chinese Railway, 7 (2006), 53-55.
[5] Chen, G. Z., Xiao, K.Z., Jiang, B.Q.: *Manual of Foundry Defect and Countermeasure*, China Machine Press, Beijing, 2007.
[6] Wang, D., Li, Y.H., Guo, G.S.: *The feeding mechanism and mathematical model during solidification of casting*, Foundry, 45 (1996), 13-16.
[7] Li, R., Mao, X.M., Liu, B.C.: *Application of layer-by-layer solidification principle to optimization of large chain wheel foundry technology*, Journal of Shanghai University (English Edition), 7(2003), 294-300.
[8] TB/T 1013-1999, *Standard Specification of cast-steel wheel*, China Railway Publishing House, Beijing , 1999 (in Chinese).
[9] Zhang, B., Lu, G.J., Fu, X.Q.: *Atlas of Failure Analysis and Damage of Wheels and tyres in Rail*, China Railway Publishing House, Beijing, 2002 (in Chinese).